Theory of Zener-phonon resonances in the transport of two-band semiconductor superlattices



2000 J. Phys.: Condens. Matter 12 8467

(http://iopscience.iop.org/0953-8984/12/39/309)

J. Phys.: Condens. Matter **12** (2000) 8467–8473. Printed in the UK PII: S0953-8984(00)16035-7

# Theory of Zener-phonon resonances in the transport of two-band semiconductor superlattices

P Kleinert

Paul-Drude-Institut für Festkörperelektronik, Hausvogteiplatz 5–7, 10117 Berlin, Germany

E-mail: kl@pdi-berlin.de

Received 2 August 2000

**Abstract.** The influence of electron–phonon scattering on intersubband tunnelling in two-band semiconductor superlattices is treated on the basis of the density-matrix approach. Intracollisional field effects are accounted for. Three different types of current resonance are identified: (i) electro-phonon resonances, which are expected to appear when a multiple of the Bloch frequency $\Omega$ matches the frequency of polar-optical phonons $\omega_0$, (ii) intersubband tunnelling resonances, and (iii) Zener-phonon resonances, which depend non-analytically on the electric field strength. The latter resonances are most pronounced when the widths of the upper and lower miniband differ appreciably.

## 1. Introduction

In recent years, the non-linear transport in semiconductor superlattices (SLs) has been intensely investigated both experimentally and theoretically. The physics of biased SLs is extremely rich due to the numerous material parameters that can be controlled quite freely. Most of the interest has been caused by the need for understanding the interplay between Bloch oscillations, intersubband tunnelling, and interaction effects.

When an electric field $E$ is applied perpendicular to the SL layers, i.e., parallel to the $z$-axis, several different transport regimes are commonly distinguished. At low field strengths, there is an ohmic regime, where the current linearly increases with increasing electric field. When the electric field becomes sufficiently high ($\hbar\Omega \equiv eEd > \hbar/\tau_{eff}$, where $d$ is the SL period and $\tau_{eff}$ an effective scattering time), another transport mechanism leads to negative differential conductivity (NDC). In this regime, the carriers become increasingly localized in space, so the energy levels of the Wannier–Stark (WS) ladder are resolved. NDC arises because electrons accelerated parallel to the SL axis probe the negative-effective-mass region of the miniband. In this case, carrier transport is only possible via inelastic-scattering-induced hopping-like transitions between different WS levels. Electro-phonon resonances were predicted to occur [1–3]. These resonant-type current anomalies are due to intracollisional field effects (ICFEs) [1] and have no analogy in a semiclassical approach. To our knowledge, electro-phonon resonances have been observed in narrow-band semiconductors [4, 5], but not yet in SL transport. The observation of this interesting quantum effect in SL transport is difficult because of the large current density, which leads to the formation of electric field domains.

With further increasing strength, the field may even influence intersubband transitions. In this third transport region, intersubband tunnelling resonances are expected to appear in the

0953-8984/00/398467+07$30.00  

current density. In this transport regime, the current still exhibits hopping-like character, so scattering remains essential. Both the linewidth of the tunnelling resonance and a possible shift of its position are due to scattering. It is the objective of our paper to study the influence of inelastic scattering on intersubband tunnelling in two-band SLs. To accomplish this task, ICFEs have to be taken into account.

## 2. Theory

For a homogeneous field distribution, the current density perpendicular to the SL layers is calculated from the subband distribution functions $f_\nu^\nu(\boldsymbol{k})$ ($\nu = 1, 2$) via the equation [6]

$$j_z = -\frac{en}{\hbar}\sum_{\boldsymbol{k},\nu}\varepsilon_\nu(k_z)\frac{\partial f_\nu^\nu(\boldsymbol{k})}{\partial k_z}. \tag{1}$$

Here $n$ denotes the electron density. The dispersion relations of the two-band SL for the lower ($\nu = 1$) and upper ($\nu = 2$) minibands are given by

$$\varepsilon_1(\boldsymbol{k}) = \varepsilon(\boldsymbol{k}_\perp) + \frac{\Delta_1}{2}(1 - \cos(k_z d)) \tag{2}$$

$$\varepsilon_2(\boldsymbol{k}) = \varepsilon(\boldsymbol{k}_\perp) + \varepsilon_g + \Delta_1 + \frac{\Delta_2}{2}(1 + \cos(k_z d)) \tag{3}$$

where $\Delta_1$ ($\Delta_2$) are the widths of the lower (upper) minibands and $\varepsilon_g$ the gap energy at zero electric field. We assume equal effective masses for the lateral electron motion in both minibands described by the dispersion relation $\varepsilon(\boldsymbol{k}_\perp)$.

The current density (1) is composed of two different contributions $j_z^{(t)}$ and $j_z^{(s)}$. The tunnelling part $j_z^{(t)}$ is proportional to the dipole matrix element and is sizable only in the vicinity of the intersubband resonance. In this paper, we will focus on the second contribution $j_z^{(s)}$, which is scattering induced and exhibits a number of interesting peculiarities. Starting from the kinetic equations for the subband distribution functions, the scattering-induced current can be expressed as [6]

$$\begin{aligned} j_z^{(s)} = -\frac{n}{E}\sum_{\boldsymbol{k},\boldsymbol{k}'}\big\{&\varepsilon_1(k_z) f_1^1(\boldsymbol{k}') W_{11}^{11}(\boldsymbol{k}', \boldsymbol{k}) + \varepsilon_2(k_z) f_2^2(\boldsymbol{k}') W_{22}^{22}(\boldsymbol{k}', \boldsymbol{k}) \\ &+ \varepsilon_1(k_z) f_2^2(\boldsymbol{k}') W_{21}^{21}(\boldsymbol{k}', \boldsymbol{k}) + \varepsilon_2(k_z) f_1^1(\boldsymbol{k}') W_{12}^{12}(\boldsymbol{k}', \boldsymbol{k})\big\} \end{aligned} \tag{4}$$

where $W_{\nu\nu'}^{\nu\nu'}(\boldsymbol{k}', \boldsymbol{k})$ denote the scattering probabilities, which depend on the electric field. The equations for these quantities are given in appendix A.

At high electric fields ($\Omega\tau_{eff} \gg 1$), we find all the WS states to be strongly confined in the direction along the SL axis. In this case, we will conveniently employ the Stark ladder representation of the distribution functions [7]

$$f_\nu^\nu(\boldsymbol{k}) = \sum_{l=-\infty}^{\infty} \mathrm{e}^{\mathrm{i}lk_z d} f_\nu^\nu(\boldsymbol{k}_\perp, l) \tag{5}$$

which is nothing but a discrete Fourier transformation of the distribution function. In the high-field limit considered, the main contributions to the right-hand side of equation (4) are supplied by the lateral distribution functions

$$f_\nu^\nu(\boldsymbol{k}_\perp, l = 0) = \sum_{k_z} f_\nu^\nu(\boldsymbol{k}).$$

These non-equilibrium distributions have to be calculated from a coupled set of kinetic equations. However, in the sequential tunnelling regime, one can avoid this additional complication by taking Boltzmann-type functions of the form

$$f_\nu^\nu(\varepsilon(\boldsymbol{k}_\perp), l=0) = \frac{2\pi\hbar^2}{mk_BT} F_\nu \exp\left(-\frac{\varepsilon(\boldsymbol{k}_\perp)}{k_BT}\right) \tag{6}$$

where $F_\nu$ denotes the global occupation of the miniband $\nu = 1, 2$. The lateral distribution function in equation (6) depends on the wave vector $\boldsymbol{k}_\perp$ only via the energy $\varepsilon(\boldsymbol{k}_\perp)$. For simplicity, the occupation numbers $F_\nu$ are calculated in the relaxation-time approximation. Following the approach outlined in reference [6], we obtain

$$F_2 = A/(2A + \tau/\tau_{21}) \qquad \text{and} \qquad F_1 = 1 - F_2 \tag{7}$$

with

$$A = 2Q_{12}^2(\Omega\tau)^2 \sum_{l=-\infty}^{\infty} \frac{J_l^2((\Delta_1+\Delta_2)/2\hbar\Omega)}{(l\Omega\tau - \omega_g\tau)^2 + 1}. \tag{8}$$

$Q_{12}$ is the dipole matrix element, $J_l$ the Bessel function, and $\hbar\omega_g = \varepsilon_g + (\Delta_1 + \Delta_2)/2$ an effective energy gap. Carrier recombination is described by the scattering time $\tau_{21}$, and the width of the tunnelling resonance is determined by $\tau$. At the tunnelling resonance $\Omega = \omega_g$, a sizable redistribution of carriers may occur. However, according to equations (7) and (8), a global population inversion is not possible in the model of a two-band SL considered.

The scattering-induced current density can be calculated from equations (2) to (8). We restrict ourselves to consideration of the case of constant coupling matrix elements. Our model approximation, which we have adopted to describe coupled Zener-phonon resonances, has the advantage of simplicity and exhibits all basic physical features. In the derivation of an expression for the current density, we used analytical results for $k_z$-integrals presented in appendix B. For the scattering-induced intrasubband current contribution, it follows that

$$j_\nu^{(intra)}/j_0^{(intra)} = \frac{F_\nu}{1-\mathrm{e}^{-\beta}} \sum_{l=-\infty}^{\infty} l f_l\left(\frac{\Delta_\nu}{\hbar\Omega}\right)\left[G(l\Omega-\omega_0) + \mathrm{e}^{-\beta}G(l\Omega+\omega_0)\right] \tag{9}$$

where $\beta = \hbar\omega_0/k_BT$ and $f_l(\Delta_\nu/\hbar\Omega)$ is defined by equation (B.2). The resonant-type character of the $I$–$V$ characteristics is expressed by step functions entering the definition of $G(x)$:

$$G(x) = \Theta(x) + \Theta(-x)\exp\left(\frac{x}{k_BT}\right). \tag{10}$$

A constant intrasubband reference current density $j_0^{(intra)}$ was introduced, which is given by $enm\omega_0^2|\gamma_{\nu\nu}|^2/\hbar^3$. The current density in equation (9) implicitly depends on intersubband effects via the field-dependent carrier occupation numbers $F_\nu$. However, there is also a scattering-induced current contribution, which is directly related to intersubband transitions. This specific current density is given by

$$\begin{aligned} j_{\nu\bar\nu}^{(inter)}/j_0^{(inter)} = {} & \frac{1}{1-\mathrm{e}^{-\beta}} \sum_{l,l'=-\infty}^{\infty} l J_l^2\left(\frac{\Delta_\nu}{2\hbar\Omega}\right) J_{l'}^2\left(\frac{\Delta_{\bar\nu}}{2\hbar\Omega}\right) \\ & \times \left\{F_1\left[G(-\omega_g + (l+l')\Omega - \omega_0) + \mathrm{e}^{-\beta}G(-\omega_g + (l+l')\Omega + \omega_0)\right]\right. \\ & \left. - F_2\left[G(\omega_g - (l+l')\Omega - \omega_0) + \mathrm{e}^{-\beta}G(\omega_g - (l+l')\Omega + \omega_0)\right]\right\} \end{aligned} \tag{11}$$

where $\bar\nu = 2$ if $\nu = 1$ and vice versa. The intersubband reference current density is expressed by $j_0^{(inter)} = enm\omega_0^2|\gamma_{\nu\bar\nu}|^2/\hbar^3$.

## 3. Numerical results and discussion

The scattering-induced current density of the two-band SL has been calculated from equations (9) and (11) by taking into account the field-dependent inelastic scattering on polar-optical phonons. Our approach is valid in the region of high electric fields, when $\Omega\tau_{eff} > 1$ and $\varepsilon_g > \Delta_v$ are satisfied. To reproduce additionally the linearly increasing part of the $I$–$V$ characteristics at low electric field strengths, we have to give up our restriction to the lowest order Fourier component of the distribution function in the expression for the current density. However, the most interesting carrier transitions take place at high electric fields, when only a few WS levels participate.

Figure 1 shows numerical results for the relative current density as a function of the electric field. A set of three different current resonances can be identified. At comparatively low electric fields, there are electro-phonon resonances at $l\Omega = \omega_0$ (indicated by vertical dash–dotted lines, $l = 1, 2, 3, \ldots$), which are strongly enhanced at low temperatures. In addition, there is a second group of current maxima marked by dashed lines, which appear when a multiple of the Bloch energy matches the effective gap ($l\Omega = \omega_g$). For the hopping-type transport mechanism considered, these structures arise from the field-dependent redistribution of the carrier density. The inset of figure 1 displays the occupation of the lower (solid line) and upper miniband (dashed line) as functions of the electric field. For the set of parameters

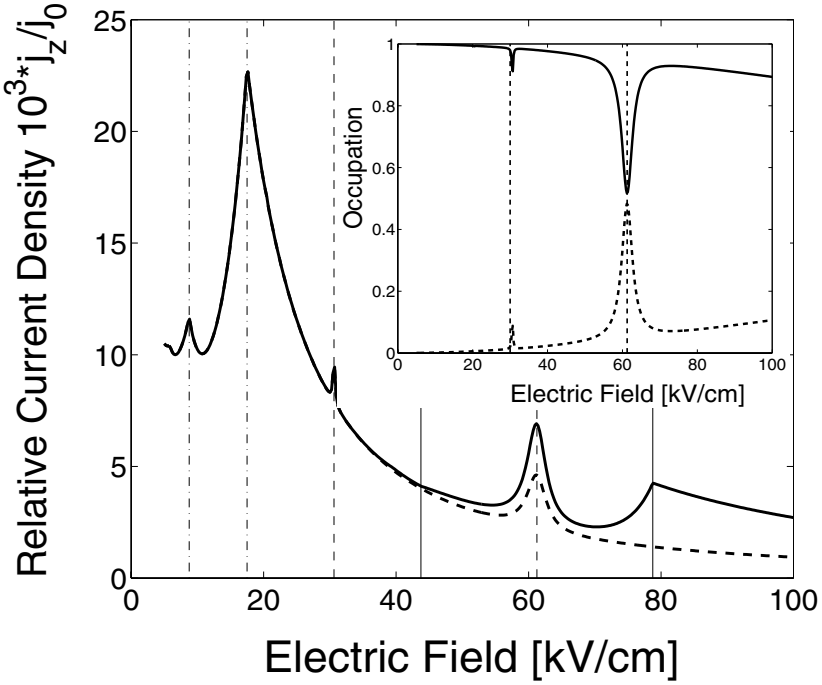


**Figure 1.** The electric field dependence of the relative current density for $\varepsilon_g = 100$ meV, $\Delta_1 = 15$ meV, $\Delta_2 = 30$ meV, and $T = 77$ K (solid line). The carrier occupation has been calculated from equations (7) and (8) using the scattering times $\tau = 1$ ps and $\tau_{21} = 1$ ps. Electro-phonon, intersubband, and Zener-phonon resonances are marked by dash–dotted, dashed, and solid vertical lines, respectively. The intrasubband part of the current density is shown by the dashed line. The inset displays the field-dependent carrier occupation of the lower (solid line) and upper miniband (dashed line). The SL period is given by $d = 20$ nm.

used in the calculation, the carrier densities almost equilibrate at the intersubband resonance $\Omega = \omega_g$, giving rise to a corresponding current maximum. Finally, one identifies in the $I$–$V$ characteristics so-called Zener-phonon resonances, which group around the intersubband resonance and appear at $l\Omega = \omega_g \pm \omega_0$ (vertical solid lines). These structures are solely due to intersubband transitions as seen from the dashed line, which depicts the intrasubband current contribution alone. The peak of the dashed line at 60 kV cm$^{-1}$ is due to the resonance in the carrier occupation. Electro-phonon and Zener-phonon resonances are very similar. Both current anomalies exhibit a non-analytic field dependence described by step functions, since the dispersion of polar-optical phonons has been neglected. The quantum-mechanical origins of both current anomalies are ICFEs. However, there is also a striking discrepancy between electro-phonon and Zener-phonon resonances. As an interminiband effect, Zener-phonon resonances depend on the properties of both minibands and are most pronounced when the widths of the lower and upper minibands differ remarkably. In contrast, electro-phonon resonances belong to a single miniband and do not probe interminiband properties. Therefore, the conditions for an experimental verification of Zener-phonon and electro-phonon resonances are quite different.

Figure 2 shows the $I$–$V$ characteristics for $T = 300$ K and a lower miniband with a smaller width. In this case, the electro-phonon resonances almost disappear, whereas intersubband resonances still persist. This is in line with the expectation of tunnelling resonances depending only weakly on temperature.

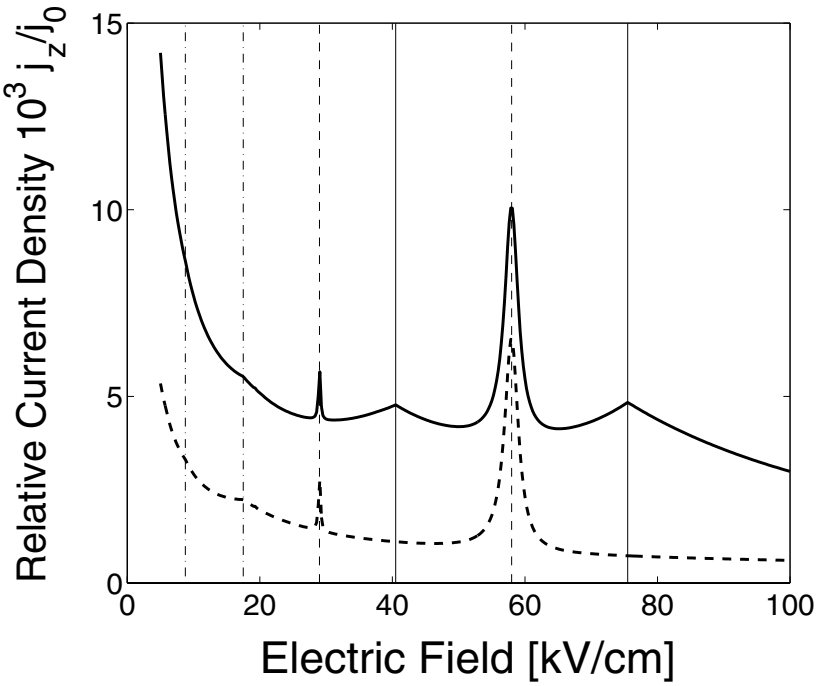


**Figure 2.** Electric field dependence of the relative current density for $\varepsilon_g = 100$ meV, $\Delta_1 = 2$ meV, $\Delta_2 = 30$ meV, and $T = 300$ K (solid line). The scattering times are $\tau = 1$ ps and $\tau_{21} = 1$ ps. The intrasubband contribution of the current density is shown by the dashed line. Electro-phonon, intersubband, and Zener-phonon resonances are marked by dash–dotted, dashed, and solid vertical lines, respectively.

## 4. Summary

On the basis of the density-matrix approach, we calculated the current density of two-band SLs by taking into account ICFEs. Besides a current maximum at the intersubband resonance $\Omega = \omega_g$, we identified two groups of quantum-mechanical current anomalies, namely so-called electro-phonon and Zener-phonon resonances, respectively. Both kinds of non-analytic current anomaly are very similar. They result from ICFEs and are described by the step functions. Nevertheless, there are also remarkable discrepancies between them as regards their dependences on temperature and the widths of the minibands. We expect our theoretical prediction to stimulate experimental studies of scattering-induced Zener-phonon current resonances in the SL transport.

## Acknowledgments

The author would like to acknowledge discussions with V V Bryksin and partial financial support by the Deutsches Zentrum für Luft- und Raumfahrt.

## Appendix A

To lowest order in the electron–phonon coupling constant, only the scattering probabilities $W_{11}^{11}$, $W_{22}^{22}$, $W_{12}^{12}$, and $W_{21}^{21}$ have to be taken into account [6]. The intrasubband contribution consists of two parts

$$\begin{aligned}
W_{11}^{11}(\boldsymbol{k}',\boldsymbol{k}) &= w_{11}^{11}(\boldsymbol{k}',\boldsymbol{k}) + \widetilde{W}_{11}^{11}(\boldsymbol{k}',\boldsymbol{k}) \\
&= \frac{2}{\hbar^2}\,\mathrm{Re}\sum_{\boldsymbol{q}}\omega_{\boldsymbol{q}}|\gamma_{11}(\boldsymbol{k},\boldsymbol{q})|^2 \\
&\quad\times\int_0^\infty \mathrm{d}t\;\mathrm{e}^{-st}\exp\left\{\frac{\mathrm{i}}{\hbar}\int_0^t \mathrm{d}\tau\;\left[\varepsilon_1(\boldsymbol{k}+\boldsymbol{q}-\boldsymbol{F}\tau)-\varepsilon_1(\boldsymbol{k}-\boldsymbol{F}\tau)\right]\right\} \\
&\quad\times\left\{\delta_{\boldsymbol{k}',\boldsymbol{k}+\boldsymbol{q}-\boldsymbol{F}t}\left[(N_{\boldsymbol{q}}+1)\mathrm{e}^{-\mathrm{i}\omega_{\boldsymbol{q}}t}+N_{\boldsymbol{q}}\mathrm{e}^{\mathrm{i}\omega_{\boldsymbol{q}}t}\right]\right. \\
&\quad\left.-\,\delta_{\boldsymbol{k}',\boldsymbol{k}-\boldsymbol{F}t}\left[(N_{\boldsymbol{q}}+1)\mathrm{e}^{\mathrm{i}\omega_{\boldsymbol{q}}t}+N_{\boldsymbol{q}}\mathrm{e}^{-\mathrm{i}\omega_{\boldsymbol{q}}t}\right]\right\} \\
&\quad-\frac{2}{\hbar^2}\,\mathrm{Re}\sum_{\boldsymbol{q}}\omega_{\boldsymbol{q}}|\gamma_{21}(\boldsymbol{k},\boldsymbol{q})|^2 \\
&\quad\times\int_0^\infty \mathrm{d}t\;\mathrm{e}^{-st}\exp\left\{\frac{\mathrm{i}}{\hbar}\int_0^t \mathrm{d}\tau\;\left[\varepsilon_2(\boldsymbol{k}+\boldsymbol{q}-\boldsymbol{F}\tau)-\varepsilon_1(\boldsymbol{k}-\boldsymbol{F}\tau)\right]\right\} \\
&\quad\times\delta_{\boldsymbol{k}',\boldsymbol{k}-\boldsymbol{F}t}\left[(N_{\boldsymbol{q}}+1)\mathrm{e}^{\mathrm{i}\omega_{\boldsymbol{q}}t}+N_{\boldsymbol{q}}\mathrm{e}^{-\mathrm{i}\omega_{\boldsymbol{q}}t}\right] \qquad \text{(A.1)}
\end{aligned}$$

where $\boldsymbol{F} = e\boldsymbol{E}/\hbar$. $W_{22}^{22}$ is obtained from this equation by exchanging the indices 1 and 2. The electron–phonon coupling constants are denoted by $\gamma_{\nu\nu'}$. We introduced a phenomenological damping parameter $s$ and the Bose distribution function $N_{\boldsymbol{q}}$. The intersubband scattering probability $W_{12}^{12}$ is given by

$$\begin{aligned}
W_{12}^{12}(\boldsymbol{k}',\boldsymbol{k}) &= \frac{2}{\hbar^2}\,\mathrm{Re}\sum_{\boldsymbol{q}}\omega_{\boldsymbol{q}}|\gamma_{12}(\boldsymbol{k},\boldsymbol{q})|^2 \\
&\quad\times\int_0^\infty \mathrm{d}t\;\mathrm{e}^{-st}\exp\left\{\frac{\mathrm{i}}{\hbar}\int_0^t \mathrm{d}\tau\;\left[\varepsilon_1(\boldsymbol{k}+\boldsymbol{q}-\boldsymbol{F}\tau)-\varepsilon_2(\boldsymbol{k}-\boldsymbol{F}\tau)\right]\right\} \\
&\quad\times\delta_{\boldsymbol{k}',\boldsymbol{k}+\boldsymbol{q}-\boldsymbol{F}t}\left[(N_{\boldsymbol{q}}+1)\mathrm{e}^{-\mathrm{i}\omega_{\boldsymbol{q}}t}+N_{\boldsymbol{q}}\mathrm{e}^{\mathrm{i}\omega_{\boldsymbol{q}}t}\right]. \qquad \text{(A.2)}
\end{aligned}$$

## Appendix B

In the derivation of our final equations (9) and (11) for the scattering-induced current density, we exploited the following analytical results for the $k_z$-integrals:

$$\sum_{k_z,q_z}\left[\varepsilon_1\left(k_z+\frac{q_z}{2}\right)-\varepsilon_1\left(k_z-\frac{q_z}{2}\right)\right] \times \exp\left\{\frac{\mathrm{i}}{\hbar}\int_0^t \mathrm{d}\tau\ \left[\varepsilon_1\left(k_z+\frac{q_z}{2}-F\tau\right)-\varepsilon_1\left(k_z-\frac{q_z}{2}-F\tau\right)\right]\right\} = \sum_{l=-\infty}^{\infty} l\hbar\Omega \mathrm{e}^{\mathrm{i}l\Omega t} f_l\left(\frac{\Delta_1}{\hbar\Omega}\right) \tag{B.1}$$

where

$$f_l\left(\frac{\Delta}{\hbar\Omega}\right)=\frac{1}{\pi}\int_0^{\pi}\mathrm{d}z\ J_l^2\left(\frac{\Delta}{\hbar\Omega}\sin z\right) \tag{B.2}$$

and

$$\sum_{k_z,q_z}\varepsilon_1(k_z)\exp\left\{\frac{\mathrm{i}}{\hbar}\int_0^t \mathrm{d}\tau\ \left[\varepsilon_2\left(k_z+\frac{q_z}{2}-F\tau\right)-\varepsilon_1\left(k_z-\frac{q_z}{2}-F\tau\right)\right]\right\} = \sum_{l=-\infty}^{\infty} l\hbar\Omega \mathrm{e}^{-\mathrm{i}l\Omega t} J_l^2\left(\frac{\Delta_1}{2\hbar\Omega}\right)\sum_{l'=-\infty}^{\infty}\mathrm{e}^{-\mathrm{i}l'\Omega t}J_{l'}^2\left(\frac{\Delta_2}{2\hbar\Omega}\right). \tag{B.3}$$

Using these results, the calculation of the $t$-integral in equations (A.1) and (A.2) becomes straightforward.

## References


[1] Bryksin V V and Kleinert P 1997 *J. Phys.: Condens. Matter* **9** 7403
[2] Rott S, Binder P, Linder N and Döhler G H 1998 *Physica* E **2** 511
[3] Wacker A *et al* 1999 *Phys. Rev. Lett.* **83** 836
[4] Maekawa S 1970 *Phys. Rev. Lett.* **24** 1175
[5] May D and Vecht A 1975 *J. Phys. C: Solid State Phys.* **8** L505
[6] Bryksin V V, Woloschin V C and Rajtzev A W 1980 *Fiz. Tverd. Tela* **22** 3076 (Engl. Transl. 1980 *Sov. Phys.–Solid State* **22** 1796)
[7] Bryksin V V and Firsov Y A 1971 *Zh. Eksp. Teor. Fiz.* **61** 2373 (Engl. Transl. 1971 *Sov. Phys.–JETP* **34** 1272)